PERGAMON International Journal of Multiphase Flow 25 (1999) 175–182

International Journal of Multiphase Flow

Brief communication

Three-dimensional oscillation of bubbly flow in a vertical cylinder

K. Kuwagi, H. Ozoe *

Institute of Advanced Material Study, Kyushu University, Kasuga, Fukuoka 816, Japan

Received 12 June 1997; received in revised form 13 March 1998

1. Introduction

The gas–liquid, two-phase flow problems arise in many industrial processes, and appropriate model equations need to be established. Although many model equations (e.g. Kataoka and Tomiyama, 1993) have been suggested, there still appears to be inconsistencies in the evaluation between various models. Therefore, it is essential to study the flow structure sufficiently.

A cylindrical vessel is often utilized as actual industrial equipment, and many investigations have been carried out for two-phase flow in a vertical cylinder. For example, Rietema and Ottengraf (1970) experimentally analyzed laminar liquid circulation and bubble street formation, and Celik and Wang (1994) carried out numerical simulations for the problem. Durst et al. (1986) carried out both experimental and numerical simulation. However, most of these approaches are two-dimensional (2D).

On the other hand, two-phase flow has a characteristic unsteadiness. For bubbly flow, it is well known that a bubble plume often sways (Matsumoto and Murai, 1995). Becker et al. (1994) and Tomiyama et al. (1994) have carried out the calculation and experiment for the unsteady, 2D gas–liquid flow in rectangular bubble columns with good agreement between them. However, it is necessary to employ a three-dimensional (3D) model to solve such a flow in a vertical cylinder. Three-dimensional two-phase flow in a cylinder has not yet been analyzed sufficiently, because of the computational difficulty.

In this paper, both experimental and numerical analyses were carried out for the two-phase flow problem in a vertical cylinder. Both flow visualization and laser-Doppler measurements were carried out. Then, fully 3D numerical analyses were carried out for comparison.

* Corresponding author.

PII: S0301-9322(98)00039-1

2. Experiment

The experimental set-up is shown schematically in Fig. 1. The inner radius of the acrylic cylinder is 80 mm. The cylinder was filled with tap water to a height of 200 mm (Gofuku et al. 1993).

The air bubbles were injected through the central bottom porous wall of a cylinder into a water tank with the mass flow rate $Q = 1.67 \times 10^{-6}$ m^3/s. Here, the bubbles were generated by the compressed air through a glass filter (the radius $r_{in} = 10$ mm, the standard maximum diameter of the hole is 100–150 μm).

Firstly, to understand the whole flow pattern, it was visualized with aluminum particles dispersed and illuminated by a slit light from a projector. In order to have greater sight, the cylinder was surrounded by a square acrylic box, and the tap water was filled between them. The flow patterns were taken by a camera, where the shutter of the camera was open for 1 s.

Secondly, the velocity profile of the liquid phase was measured by a laser-Doppler velocimeter (LDV) with a forward scattering method. Data samples of 256 pieces were taken at each point.

3. Theoretical analyses

3.1. Model equation

For numerical analysis, the following assumptions were utilized.

1. The mass transfer between liquid and gas phases does not exist.
2. The liquid and gas phases are treated as incompressible fluid.
3. The temperature in the domain is constant and uniform.

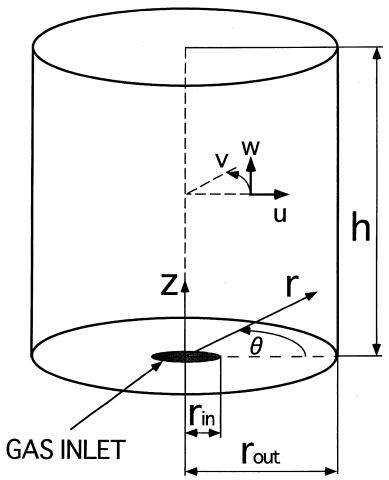

Fig. 1. Problem schematic $h = 200$ mm, $r_{out} = 80$ mm, $r_{in} = 10$ mm, pore size of gas inlet $= 100$–150 μm.

4. The coalescence and fragmentation of the bubbles are not considered.
5. No turbulence models are employed.

From the above assumptions, the governing equations become as follows. The continuity equation is as follows.

$$\frac{\partial \epsilon_k}{\partial t} + \nabla \cdot (\epsilon_k \, \mathbf{v}_k) = 0, \tag{1}$$

$$\epsilon_{\mathrm{L}} + \epsilon_{\mathrm{G}} = 1. \tag{2}$$

Following Durst et al. (1986), with an addition of a virtual mass force term, the momentum equation for the liquid phase becomes:

$$\epsilon_{\mathrm{L}} \rho_{\mathrm{L}} \frac{D_{\mathrm{L}} \mathbf{v}_{\mathrm{L}}}{Dt} = -\epsilon_{\mathrm{L}} \nabla p + \epsilon_{\mathrm{L}} \, \mathbf{F}_{\mathrm{V}} + \mathbf{F}_{\mathrm{D}} + \mathbf{F}_{\mathrm{VM}} + \mathbf{F}_{\mathrm{L}} - \rho_{\mathrm{L}} \, \mathbf{g} \, \epsilon_{\mathrm{L}}. \tag{3}$$

The momentum equation for the gas phase becomes:

$$\epsilon_{\mathrm{G}} \rho_{\mathrm{G}} \frac{D_{\mathrm{G}} \mathbf{v}_{\mathrm{G}}}{Dt} = -\epsilon_{\mathrm{G}} \nabla p - \mathbf{F}_{\mathrm{D}} - \mathbf{F}_{\mathrm{VM}} - \mathbf{F}_{\mathrm{L}} - \rho_{\mathrm{G}} \, \mathbf{g} \, \epsilon_{\mathrm{G}}, \tag{4}$$

where D_k/Dt is the material derivative following phase k. $\mathbf{F}_{\mathrm{v}}$, $\mathbf{F}_{\mathrm{D}}$, $\mathbf{F}_{\mathrm{VM}}$ and $\mathbf{F}_{\mathrm{L}}$ are viscous force, drag force, virtual mass force and lift force, respectively, as defined as follows (Drew and Lahey, 1987):

$$\mathbf{F}_{\mathrm{V}} = -[\nabla \cdot \tau_{\mathrm{L}}] \quad \text{with} \quad \mu = \mu_{\mathrm{L}}(1 + \epsilon_{\mathrm{G}}), \tag{5}$$

$$\mathbf{F}_{\mathrm{D}} = \frac{3}{4} \frac{C_{\mathrm{D}} \, \epsilon_{\mathrm{G}} \, \rho_{\mathrm{L}} \, \mathbf{v}_{\mathrm{r}} |\mathbf{v}_{\mathrm{r}}|}{d_{\mathrm{B}}}, \tag{6}$$

$$C_{\mathrm{D}} = \begin{cases} 24/Re & (Re \leq 2) \\ \dfrac{24}{Re}\left(1 + 0.15 Re^{0.687}\right) & (Re \geq 2) \end{cases}, \tag{7}$$

$$\mathbf{F}_{\mathrm{VM}} = \epsilon_{\mathrm{G}} \, \rho_{\mathrm{L}} \, C_{\mathrm{VM}} \left\{ \frac{D_{\mathrm{G}} \, \mathbf{v}_{\mathrm{G}}}{Dt} - \frac{D_{\mathrm{L}} \, \mathbf{v}_{\mathrm{L}}}{Dt} \right\}, \tag{8}$$

$$\mathbf{F}_{\mathrm{L}} = C_{\mathrm{L}} \, \rho_{\mathrm{L}} \, \epsilon_{\mathrm{G}} \, \mathbf{v}_{\mathrm{r}} \times (\nabla \times \mathbf{v}_{\mathrm{L}}), \tag{9}$$

where Re is a bubble Reynolds number ($=\rho_{\mathrm{L}} d_{\mathrm{B}} \mathbf{v}_{\mathrm{r}}/\mu_{\mathrm{L}}$), d_{B} is a bubble diameter ($=1$ mm), and $\mathbf{v}_{\mathrm{r}} = \mathbf{v}_{\mathrm{G}} - \mathbf{v}_{\mathrm{L}}$. C_{VM} is a virtual mass coefficient. For the simplicity, a virtual mass coefficient was set to 0.5, which is the value for a single spherical bubble. C_{L} is a lift force coefficient, and is set to a constant: 0.5 in this calculation.

3.2. Numerical procedure

The above momentum equations were approximated by finite difference equations. The time discretization was approximated by an explicit method, and the inertial terms by the K–K scheme (Kawamura and Kuwahara 1984). The pressure distribution was solved with the highly simplified marker and cell (HS–MAC) method. The liquid is initially static and no bubbles exist (Kuwagi and Ozoe, 1997).

The boundary conditions are as follows. For the liquid phase, the velocity on a wall is zero and the slip condition was used for a top surface. For the gas phase, the slip condition was used on a wall, and bubbles leave from a free surface immediately ($\partial u_G/\partial z = \partial v_G/\partial z = \partial w_G/\partial z = \partial \epsilon_G/\partial z = 0$).

The grid numbers are $(r \times \theta \times z) = (20 \times 36 \times 50)$. The time step is 1.09×10^{-5} s.

4. Results and discussion

Figure 2(a) shows a photograph of aluminum particles, (b) computed liquid velocity vectors, and (c) computed stream lines of the gas bubble from a bottom inlet. The flow is more or less asymmetric. Along the vertical axis of the cylinder, strong ascending velocity vectors are due to the bubble flows. In the photograph, strong rising air bubbles can be seen in the radial center region. Relatively large scale vortices can be seen outside of the rising bubbles. They are changing sizes and locations transiently. A horizontal line at $z = 0.17$ m in Fig. 2(b), corresponds to a center level of the main vortex in the photograph of Fig. 2(a). Computed

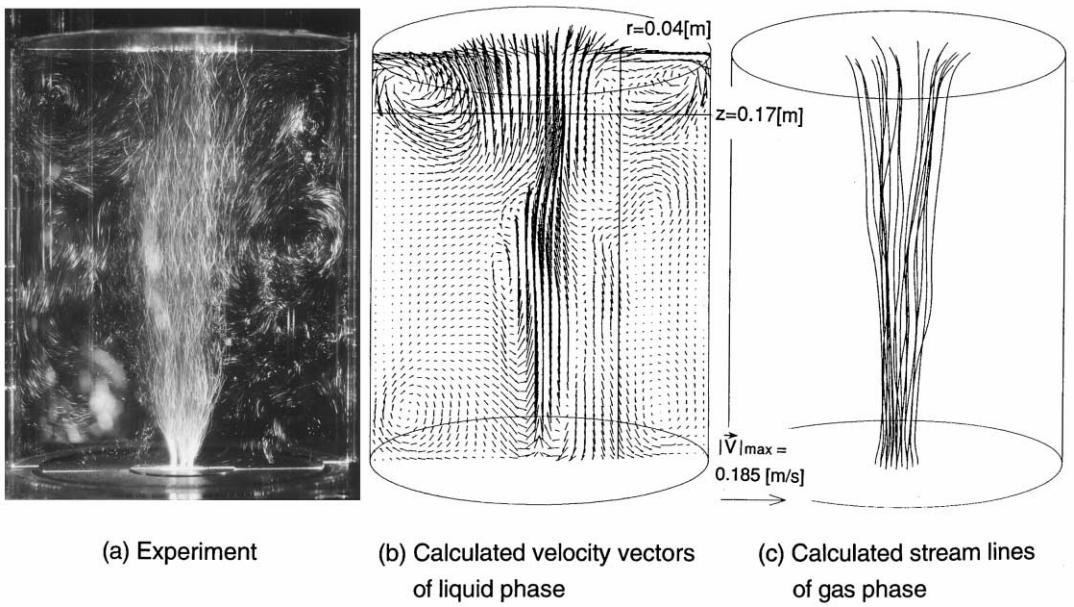

Fig. 2. Typical asymmetric flow pattern of liquid phase in a vertical section for air bubbles in a water tank. Aluminum particles were dispersed in water for flow visualization: (a) experiment; (b) calculated velocity vectors of liquid phase; and (c) calculated stream lines of gas phase.

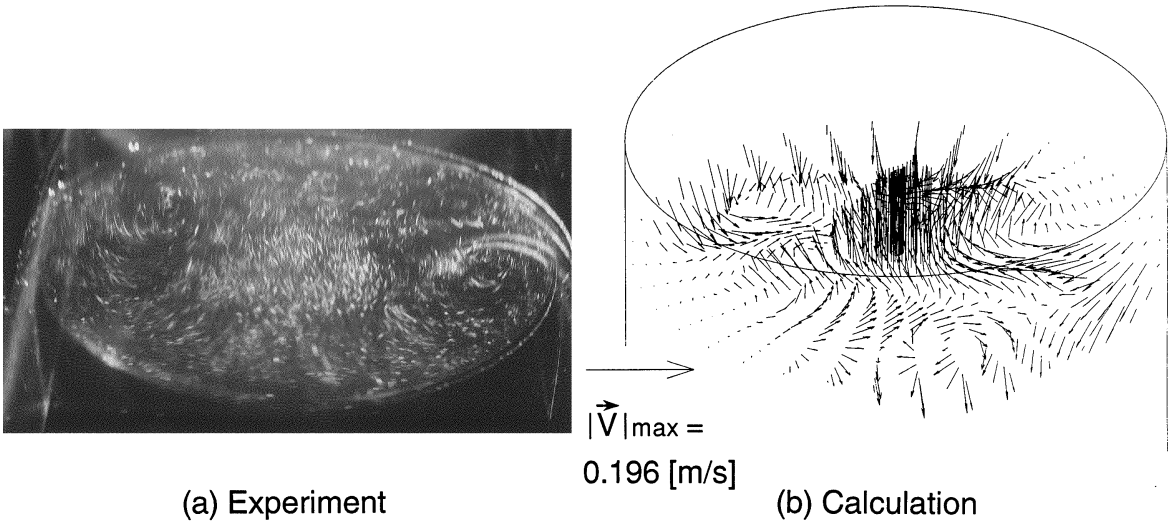

Fig. 3. Typical asymmetric flow pattern of liquid phase in a cross horizontal section at a level, $z = 0.16$ m: (a) experiment; and (b) calculation.

sizes of the main vortex may indicate the quantitative measure on the accuracy of the numerical analyses. On the other hand, although the flow of the gas phase is also asymmetric, the asymmetry is smaller than the liquid one. Fig. 3(a) shows a photograph of aluminum particles, and (b) the computed liquid velocity vectors, both in a horizontal section at $z = 0.16$ m. In the center, vertical liquid velocity vectors are due to the ascending bubbles. Similar dense white vertical lines can be seen in the photographs; even horizontal vortices can be seen in both pictures. Quite similar flow characteristics could have been obtained between these results.

Figure 4 shows both experimental and calculated radial distributions of a vertical velocity component of the liquid phase along the radial line, at $z = 0.17$ m. The data represents the value averaged over 256 samples in the experiment or 240 samples in the calculation, over a certain time period at each point. The periods are approximately 10–20 s in the experimental results, depending on the particle sampling conditions, and 13.1 s in the calculated results. The experimental profile has a re-entrant shape in the central region. A reasonably similar profile can be seen in the calculated distribution. This re-entrant shape is considered to be caused by the oscillatory flow as follows.

Figure 5 shows a trajectory of the position of the maximum vertical velocity computed between $t = 22.9$–26.2 s. The position moves in both radial and circumferential directions. Roughly, the direction is circumferential between $t = 22.9$–23.5 s and 24.5–25.9 s and radial between $t = 23.5$–24.5 s and 25.9–26.2 s.

Figure 6 shows two types of oscillatory flow pattern. The curve represents liquid or gas upward flow. When the oscillation is through a radial center as shown in Fig. 6(a), the time-averaged radial velocity profile should become something like that on the right-hand side picture. When the oscillation is rotating about the cylinder axis, as shown in Fig. 6(b), the

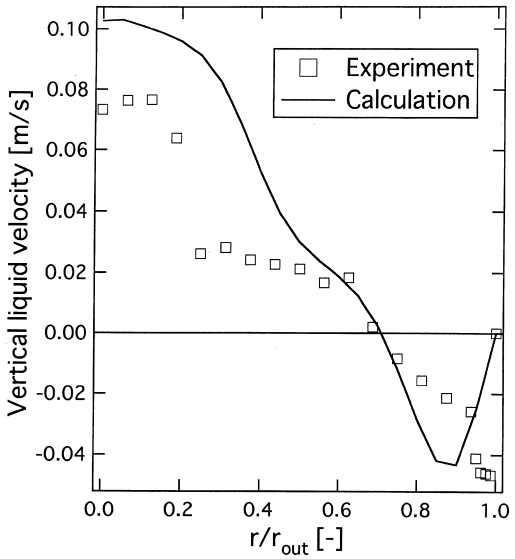

Fig. 4. Radial distribution of vertical liquid velocity at a level, $z = 0.17$ m.

time-averaged profile would become something like the re-entrant shape. In a practical case, these two oscillations would occur simultaneously.

Figure 7 shows the radial distribution of the standard deviation of the vertical liquid velocity at $z = 0.17$ m both from the experiment and from simulations. The standard deviation represents the root-mean-square (rms) value of the fluctuating velocity. The calculated distribution qualitatively agrees with the experimental one. The fluctuation is large at $r/r_{out} \leq 0.3$, small at $r/r_{out} \approx 0.3$–0.95, and again somewhat large at $r/r_{out} \approx 0.975$. The large fluctuation in the center region is caused by fluctuation of liquid flow itself and ascending bubble motion. The fluctuation close to the side wall is caused by the descending circulating liquid flow. The standard deviations close to the center have the re-entrant shape, similar to the vertical velocity itself. The distribution of a standard deviation like this profile, was also

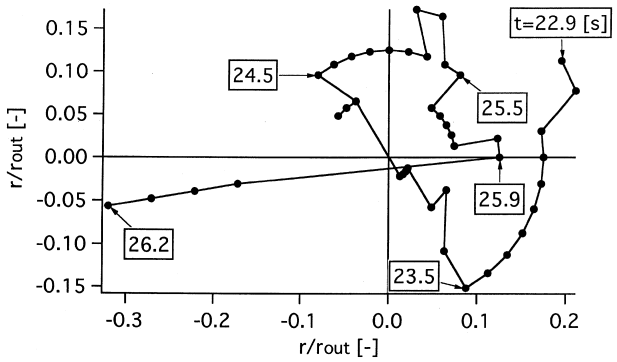

Fig. 5. A horizontal trajectory of the position of maximum vertical velocity computed between $t = 22.9$ and 26.2 s.

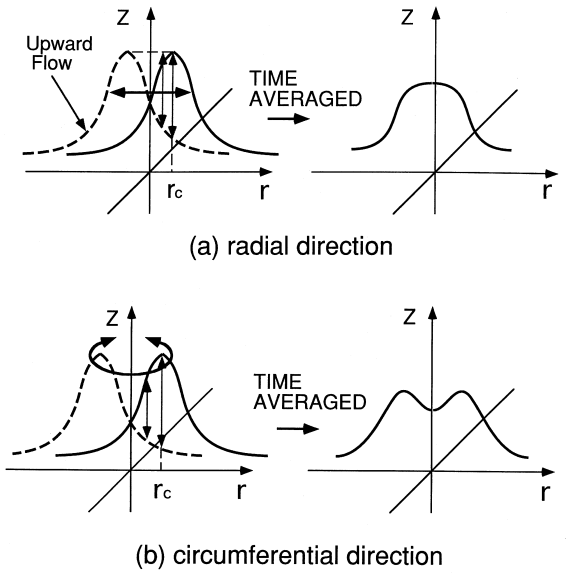

Fig. 6. Schematic of the oscillatory flow pattern: (a) radial oscillation; and (b) circumferential oscillation.

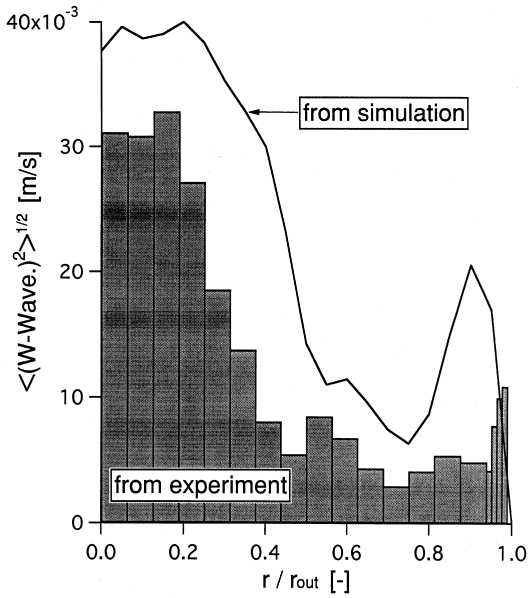

Fig. 7. Standard deviation of vertical velocity at a level, $z = 0.17$ m.

obtained by Iguchi et al. (1997) experimentally. However, peak values of the standard deviation at $r \approx r_c$ may occur for both flow models, as shown in Fig. 6.

5. Conclusions

Experimental measurements and transient 3D calculations with two-fluid model, were carried out for a two-phase flow in a vertical cylinder. The conclusions are summarized as follows:

1. The asymmetric flow was observed both in the visualized results and in the numerical results. This asymmetric flow would be caused by the oscillatory flow about the center axis of the cylindrical enclosure.
2. The radial distribution of vertical liquid velocity at $z = 0.17$ m (water height $h = 0.20$ m), became the re-entrant shape in the center region, probably because of the rotating flow about the cylinder axis.
3. The radial distribution of the standard deviation of liquid vertical velocity, also became the re-entrant shape.
4. The time-averaged radial profile of the vertical velocity may be presumed axisymmetric and 2D. However, the re-entrant shape is caused by circumferential oscillation.

References

Becker, S., Sokolichin, A., Eigenberger, G., 1994. Gas–liquid flow in bubble columns and loop reactors: Part II Comparison of detailed experiments and flow simulations. Chem. Engng Sci. 49, 5747–5762.

Celik, I., Wang, Y-Z., 1994. Numerical simulation of circulation in gas–liquid column reactors: isothermal bubbly, laminar, flow. Int. J. Multiphase Flow 20, 1053–1070.

Drew, D.A., Lahey, R.T., Jr, 1987. The virtual mass and lift force on a sphere in rotating and straining inviscid flow. Int. J. Multiphase Flow 13, 113–121.

Durst, F., Schönung, B., Selanger, K., Winter, M., 1986. Bubble-driven liquid flows. J. Fluid Mech. 170, 53–82.

Gofuku, A., Toi, T., Kataoka, I., Serizawa, A., Kojima, K., Morikawa, T., 1994. Development of a calculation code of circulation flow induced by bubble plume in a tank. Jpn. J. Multiphase flow 7, 232–240.

Iguchi, M., Okita, K., Nakatani, T., Kasai, N., 1997. Structure of turbulent round bubbling jet generated by premixed gas and liquid injection. Int. J. Multiphase Flow 23, 249–262.

Kataoka, I., Tomiyama, A., 1993. Basic equations and their mathematical feature of gas–liquid two-phase dispersed flow based on two-fluid model. Jpn. J. Multiphase Flow 7, 132–141.

Kawamura, T., Kuwahara, K., 1984. Computation of high Reynolds number flow around a circular cylinder with surface roughness. AIAA Paper 84-0340.

Kuwagi, K., Ozoe, H., 1997. Analysis of gas–liquid two-phase flow in a cylindrical vessel (comparisons of two-phase flow models and higher-order up-wind difference schemes). Kagaku Kogaku Ronbunshu 23, 861–869.

Matsumoto, Y., Murai, Y., 1995. Numerical simulation of bubble plume in a tank with free surface. Trans. Jpn. Soc. Mech. Eng. Ser. B 61, 2818–2825.

Rietema, K., Ottengraf, S.P.P., 1970. Laminar liquid circulation and bubble street formation in a gas–liquid system. Trans. Inst. Chem. Engineers 48, T54–T62.

Taylor, G.I., 1932. The viscosity of a fluid containing small drops of another fluid. Proc. Roy. Soc. A138, 41–48.

Tomiyama, A., Uegomori, S., Minagawa, H., Fukuda, T., Sakaguchi, T., 1994. Numerical analysis of bubble-induced natural circulation based on multidimensional two-fluid model. Trans. Jpn. Soc. Mech. Engng Ser. B 60, 3987–3993.